Electrochimica Acta 93 (2013) 131–136

Contents lists available at SciVerse ScienceDirect

Electrochimica Acta

journal homepage: www.elsevier.com/locate/electacta

Facile synthesis of flower-like and yarn-like α-Fe_2O_3 spherical clusters as anode materials for lithium-ion batteries

Xiao-Hang Ma, Xu-Yong Feng, Chao Song, Bang-Kun Zou, Chu-Xiong Ding, Yan Yu, Chun-Hua Chen*

CAS Key Laboratory of Materials for Energy Conversions, Department of Materials Science and Engineering, University of Science and Technology of China, Anhui, Hefei 230026, China

ARTICLE INFO

Article history:
Received 7 November 2012
Received in revised form 14 January 2013
Accepted 18 January 2013
Available online 26 January 2013

Keywords:
Iron oxide
Morphology
Electrochemical property
Anode
Lithium-ion battery

ABSTRACT

The α-Fe_2O_3 powders composed of different flower-like or yarn-like clusters are prepared by a thermal decomposition process of iron alkoxide precursors, which are obtained via a simple reaction between iron acetylacetonate and ethylene glycol in an oil bath. X-ray diffraction, thermogravimetric analysis, scanning electron microscopy, Brunauer–Emmett–Teller measurement, and galvanostatic cell cycling are employed to characterize the structures and electrochemical performance of these α-Fe_2O_3 samples. The results show that these α-Fe_2O_3 electrodes have stable cycling performance with a reversible capacity of over 800 mAh g^{-1} after 40 cycles. The sample with optimized structure shows the best rate performance with a high capacity of 622 mAh g^{-1} at the current density of 4687 mA g^{-1}. The experimental results suggest that such an α-Fe_2O_3 powder is a promising anode material for high energy-density lithium-ion batteries.

1. Introduction

Lithium-ion batteries have been widely used as power sources for different electronic devices ranging from cellular phones, digital cameras, laptop computers to hybrid-, plug-in hybrid-, and all electric vehicles. In order to meet the increasing demands for higher energy density lithium-ion batteries, we must continue to develop new generation electrode materials [1,2]. Ideal electrodes should have high specific energy density, excellent high rate performance, long cycle life, environmental friendliness and low cost. Compared to the conventional graphite anode with gravimetric and volumetric capacities of 370 mAh g^{-1} and 760 Ah L^{-1}, respectively, hematite (α-Fe_2O_3) has much higher gravimetric and volumetric capacities of 1000 mAh g^{-1} and 5300 Ah L^{-1}, respectively [3–10]. Owing also to its advantages of low cost and non-toxicity, it has attracted much attention as a high energy anode material. However, most of the reported α-Fe_2O_3 electrodes suffer from several drawbacks including poor cycling performance, a large initial irreversible capacity loss (usually over 40%), and poor rate capability due to material pulverization and slow charge diffusion during the charging and discharging process. These problems can be solved to a large extent by reducing the particle size into nanometer scales with designed favorable microstructures [11,12], because small particle sizes can not only shorten the lithium-ion diffusion distance, but also increase the contact area between the powder and the electrolyte. Various nanostructures of α-Fe_2O_3, like one-dimensional nanowires/nanotubes [13], two-dimensional flaky or thin-film structures [14], and three-dimensional hollow/porous structures [15], have been synthesized by different methods such as sol–gel process [16], electrostatic spray deposition [17], hydrothermal process [18], and template method [19]. Nevertheless, most of these methods are either time-consuming or rather complicated. Therefore, in this study, we employ a simple wet-chemical process to convert iron acetylacetonate into iron alkoxide that subsequently changes into α-Fe_2O_3 during a further heat treatment. By tailoring the reaction conditions, we can obtain the α-Fe_2O_3 particles with different nano/micro-structures. As potential anode materials for lithium-ion batteries, these powders exhibit good cycle performance and excellent rate capability.

2. Experimental

Ferric acetylacetonate ($Fe(CH_3COCHCOCH_3)_3$ or $Fe(acac)_3$) was dissolved into 100 ml ethylene glycol (EG) at 70 °C to obtain four solutions with concentrations 0.02, 0.04, 0.06 and 0.08 M, respectively. Then, they were heated during a continuous stirring in an oil bath at 180 °C for 3 h to form four yellowish suspensions. After being cooled to room temperature, the suspensions were centrifuged and washed with ethanol, and then dried at 70 °C for 12 h to obtain yellow powders in a vacuum oven. Subsequently, these powders were calcined at 500 °C for 6 h in air and cooled to room temperature. Finally, four red-colored powders were obtained.

The crystalline structures of the yellow and red powders were characterized by X-ray diffraction (XRD) using a diffractometer

* Corresponding author. Tel.: +86 551 63606971; fax: +86 551 63601592.
E-mail address: cchchen@ustc.edu.cn (C.-H. Chen).

0013-4686/$ – see front matter © 2013 Elsevier Ltd. All rights reserved.
http://dx.doi.org/10.1016/j.electacta.2013.01.096

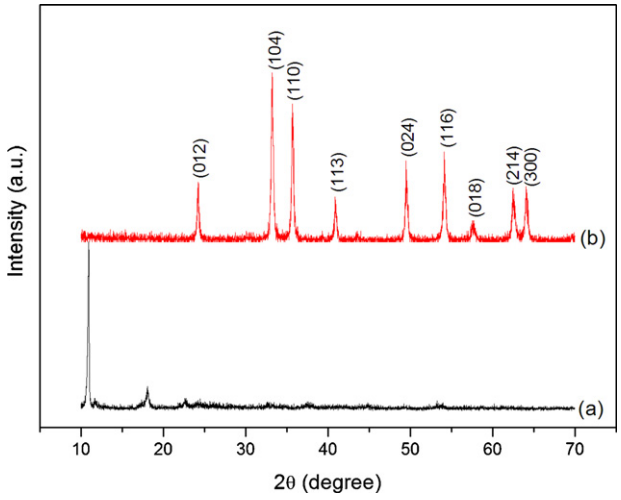

Fig. 1. XRD patterns of a yellow powder (a) and its derived red powder (b) from the 0.08 M precursor solution.

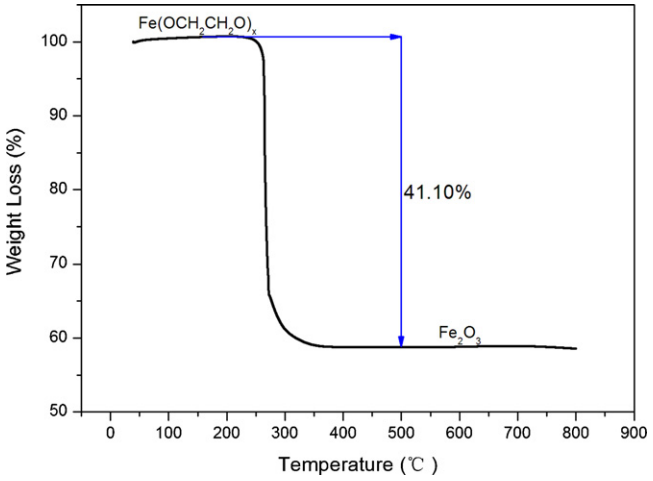

Fig. 2. TGA curve of the yellow powder made from the 0.08 M precursor solution.

(Rigaku TTR-lll, Cu Kα radiation) in the 2θ range from 10° to 70°. The thermogravimetric analysis (TGA) of the yellow powder made from the 0.08 M precursor solution was conducted with a thermal analyzer (Q5000IR, TA Instruments) in air from 25 to 800 °C at a heating rate of 5 °C min^{-1}. Both the yellow and red powders were observed under a scanning electron microscope (JSM-6390LA, JEOL). Also, their specific surface areas were measured by the Brunauer–Emmett–Teller (BET) method using nitrogen adsorption–desorption isotherms on a Surface Area Analyzer (SA3100, Beckan Coulter) and the pore size distributions were obtained from the desorption branch of the isotherms by the Barrett–Joyner–Halenda (BJH) method.

The electrochemical properties of the obtained α-Fe_2O_3 powders were evaluated in CR2032 coin cells. The α-Fe_2O_3 electrode laminates on a copper foil were prepared with acetylene black (AB) as a conductive additive and poly(vinylidene difluoride) (PVDF) as a binder (Fe_2O_3:AB:PVDF = 4:4:2 in weight). The laminates were punched into round discs with a diameter of 14 mm. The coin-cells were assembled in an argon-filled glove box (MBRAUN LABMASTER 130) with both the moisture content and oxygen levels less than 1 ppm. The α-Fe_2O_3 electrodes were used as the working electrodes and lithium metal as the counter electrode. The electrolyte was 1.0 M $LiPF_6$ in ethylene carbonate (EC) and diethyl carbonate (DEC) (EC:DEC = 1:1, v/v), and Celgard 2400 porous membrane was used as the separator. The cells were galvanostatically cycled at 25 °C on a multi-channel battery cycler (NEWWARE BTS-610) in the voltage range of 0.01–3.0 V. The impedance spectra of the cells were also measured on an electrochemical workstation (CHI 660A) in the frequency range of 0.005–100 kHz. It should be noted that the use of relatively high content of carbon (40 wt%) in the electrodes was mainly due to the rather poor electronic conductivity of iron oxide. Excessive carbon can help to improve its electrochemical performance according to our previous studies [6,20].

3. Results and discussion

Fig. 1 shows the XRD pattern of the yellow powder obtained after the oil-bath treatment of a precursor solution and that of the red powder obtained after the 500 °C calcination, respectively. It can be seen that, for the as-prepared oil-bathed powder, there is a strong peak appearing in the low-angle region (around 11° for Cu Kα radiation) (Fig. 1a), which is characteristic of the diffraction peak of a metal alkoxide [21–23]. Thus, in this study the yellow powder should be one kind of iron alkoxide, which formula can be written as $Fe(OCH_2CH_2O)_x$. According to the thermogravimetric analysis (Fig. 2), x value can be calculated as 1.35, i.e. the exact formula being $Fe(OCH_2CH_2O)_{1.35}$, which means that Fe(III) and Fe(II) coexist in the alkoxide with a molar ratio of 7:3. On the other hand, all of diffraction peaks of the calcined powder in Fig. 1b can be indexed to the standard pattern of hematite (α-Fe_2O_3) crystalline structure (JCPDS Card No. 33-0664). Because no other peaks are detected, it should be with a pure phase composition. In fact, we can draw the same conclusions for the powders obtained from precursor solutions of different concentrations.

The particle morphologies of these four α-Fe_2O_3 powders and their corresponding alkoxide powders are shown in Fig. 3. Obviously, there are no significant changes in the size and morphology between the α-Fe_2O_3 powder and its alkoxide. For the four α-Fe_2O_3 samples, they are all porous mono-dispersed spherical cluster particles composed of different shapes of primary particles. A self-assembly process must have occurred in the solutions during the oil-bath treatment. Depending on the concentration of the precursor solutions, the clusters are either with flower-like morphologies (Fig. 3a–c) from 0.02 to 0.06 M precursor solutions or a yarn-like morphology from a 0.08 M precursor solution (Fig. 3d). For the sake of simplicity, the α-Fe_2O_3 powders from 0.02, 0.04, 0.06 and 0.08 M precursor solutions are named as F02, F04, F06 and F08, respectively. More specifically, F02 consists of microspheres of about 3.0 μm, which are composed of many petal-like nanoplates with an average thickness of about 100 nm. These nanoplates interweave together forming the cluster with an open porous structure. Such a well-organized porous structure is able to facilitate electrolyte penetration into the electrode particles by providing a large contact area between the electrode material and the electrolyte, so that its electrochemical performance of the prepared materials can be improved. The benefits of this open structure are similarly applicable to the other three samples F04, F06 and F08. The secondary particle sizes of F04, F06 and F08 are about 15, 10 and 6.0 μm, respectively, with differences in the degree of openness and thickness of the nanoplates. Therefore, the overall synthesis procedure of these α-Fe_2O_3 powders can be schematically illustrated in Scheme 1.

As a representative example, the nitrogen adsorption–desorption isotherm of F08 is shown in Fig. 4. Based on the shape of the curves, the isotherm can be classified as type IV, which is characteristic of a mesoporous material [24]. The BET specific surface areas and the pore size of the samples are shown in Table 1. Obviously, the mesoporous structures of the samples can help to increase reversible Li storage capacity, but the high specific surface

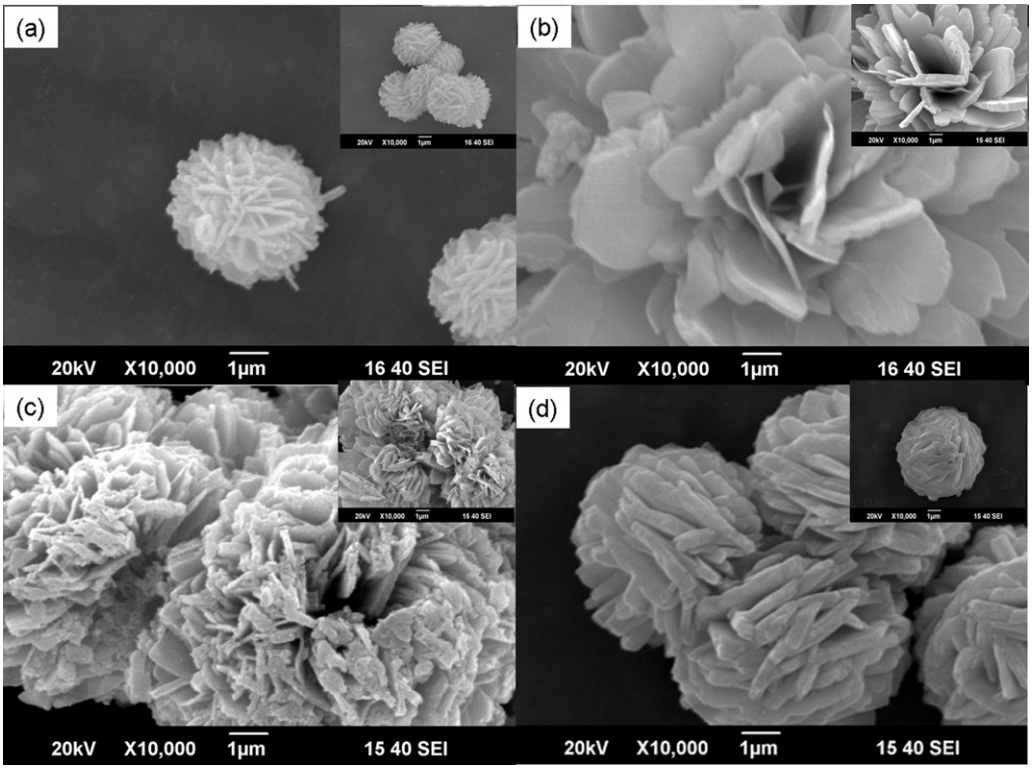

Fig. 3. SEM images of the prepared α-Fe_2O_3 powders: (a) F02; (b) F04; (c) F06; (d) F08. The inset of each image gives the SEM image of the corresponding alkoxide powder.

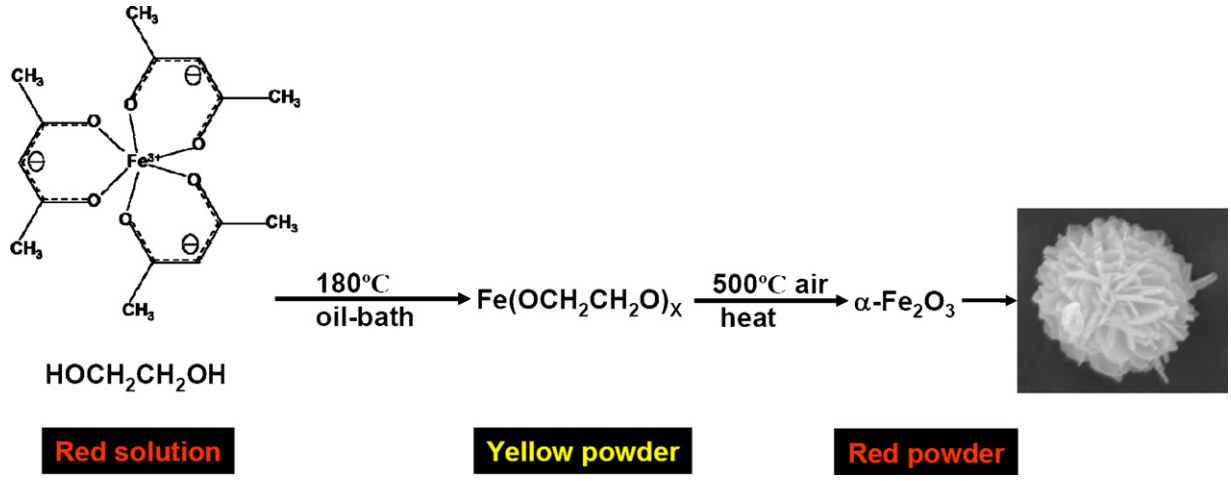

Scheme 1. Overall synthesis procedure of α-Fe_2O_3 clusters.

area is expected to consume more irreversible lithium to form solid electrolyte interphase films during the first discharge process.

The prepared α-Fe_2O_3 samples are used as anode materials for lithium-ion batteries to test the electrochemical performance as shown in Fig. 5. The voltage profiles of all of the samples show that a long voltage plateau appears at about 0.8 V during the first discharge process but disappears in the subsequent cycles. Such voltage profiles are characteristic of non-intercalation type metal-oxide electrodes [11,25–27]. For F02 as an example, in the first discharge process, there is a steep voltage drop from 3.0 to 0.75 V, which can be attributed to the partial lithiation reaction of Li intercalated into the α-Fe_2O_3 fcc lattice, i.e. $Fe_2O_3 + xLi \rightarrow Li_xFe_2O_3$. Then, an obvious voltage plateau at about 0.8 V appears, which corresponds to the conversion reaction that the Fe is driven out from the lattice to form nano-Fe clusters in a Li_2O matrix, i.e. $Li_xFe_2O_3 + (6-x)\,Li \rightarrow 2\,Fe + 3Li_2O$. The sloping part of the discharge curve between 0.8 and 0 V can be attributed to the reactions to form a gel-like film and the solid electrolyte interphase films on the surface of the working electrodes [28,30]. During the subsequent charging step, the nano-Fe clusters are oxidized back into

Table 1
The specific surface areas and the pore size of four α-Fe_2O_3 samples.

Sample	Concentration of precursor solution (M)	Morphology	BET ($m^2\,g^{-1}$)	Pore size (nm)
F02	0.02	Flower	33.65	1.16
F04	0.04	Flower	27.73	1.29
F06	0.06	Flower	26.65	1.30
F08	0.06	Flower	29.63	1.28

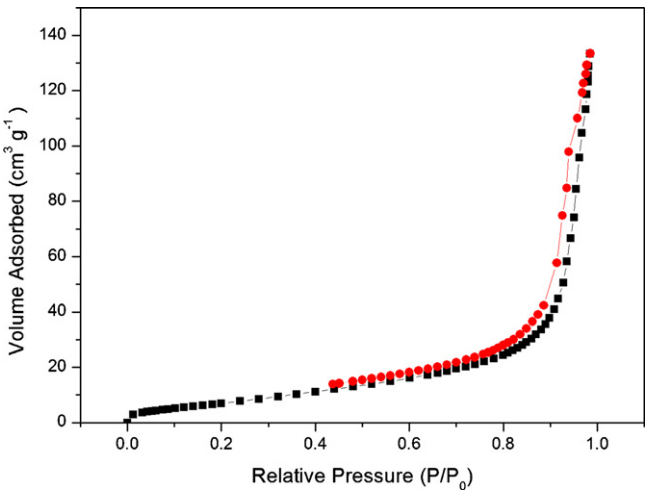

Fig. 4. Nitrogen adsorption–desorption isotherm of F08.

Fe_2O_3. The initial discharge capacities of the four samples are 1522, 1678, 1391 and 1840 mAh g^{-1}, respectively. Note that, the theoretical capacity of α-Fe_2O_3 is 1005 mAh g^{-1} in the voltage range of 0–3.0 V. The high specific capacity in the cycling process is contributed mainly by the α-Fe_2O_3 but a small portion of it is also contributed by conducting additive acetylene black (AB). The AB can supply a capacity of 255 mAh g^{-1} in the first discharge step and 150 mAh g^{-1} in the second discharge step [29]. But even if after subtracting the capacity contribution of the AB, the initial discharge capacities of the four samples are about 1267, 1423, 1136, 1585 mAh g^{-1}, respectively, which are also greater than the theoretical capacity. This phenomenon has been widely reported for transition metal oxides [28,30], which is usually ascribed to the formation of a polymeric gel-like film and possibly interfacial lithium storage. And the differences of the initial discharge capacity for the four samples are mainly due to the differences in their specific surface area and the microstructure. The initial capacity loss is 27.5%, 26.9%, 27.4%, 27.2% and the columbic efficiency of the first cycle is 67.2%, 68.2%, 68.6%, and 68.4%, respectively. It can be easily seen that the electrochemical performances of the four samples in initial two cycles are similar. Nevertheless, after 40 cycles, the capacity retention rate with respect to the discharge capacity of the second cycle is 88.51%, 74.39%, 79.45% and 70.27%, respectively, with F02 having the highest capacity retention rate.

The cycling performance and rate capability of the electrodes are shown in Fig. 6. All of the electrodes show stable cycling performance at a current of 312.5 mA g^{-1}, and the discharge capacities of the four samples are over 800 mAh g^{-1} after 40 cycles. The stable cycling performance of these samples comes from their unique hierarchical architecture. The porous and open structure of the samples has a large specific surface area that can help a quick infiltration of electrolyte and shorten the diffusion lengths for both lithium ions and electrons. Thus, compared with the electrodes

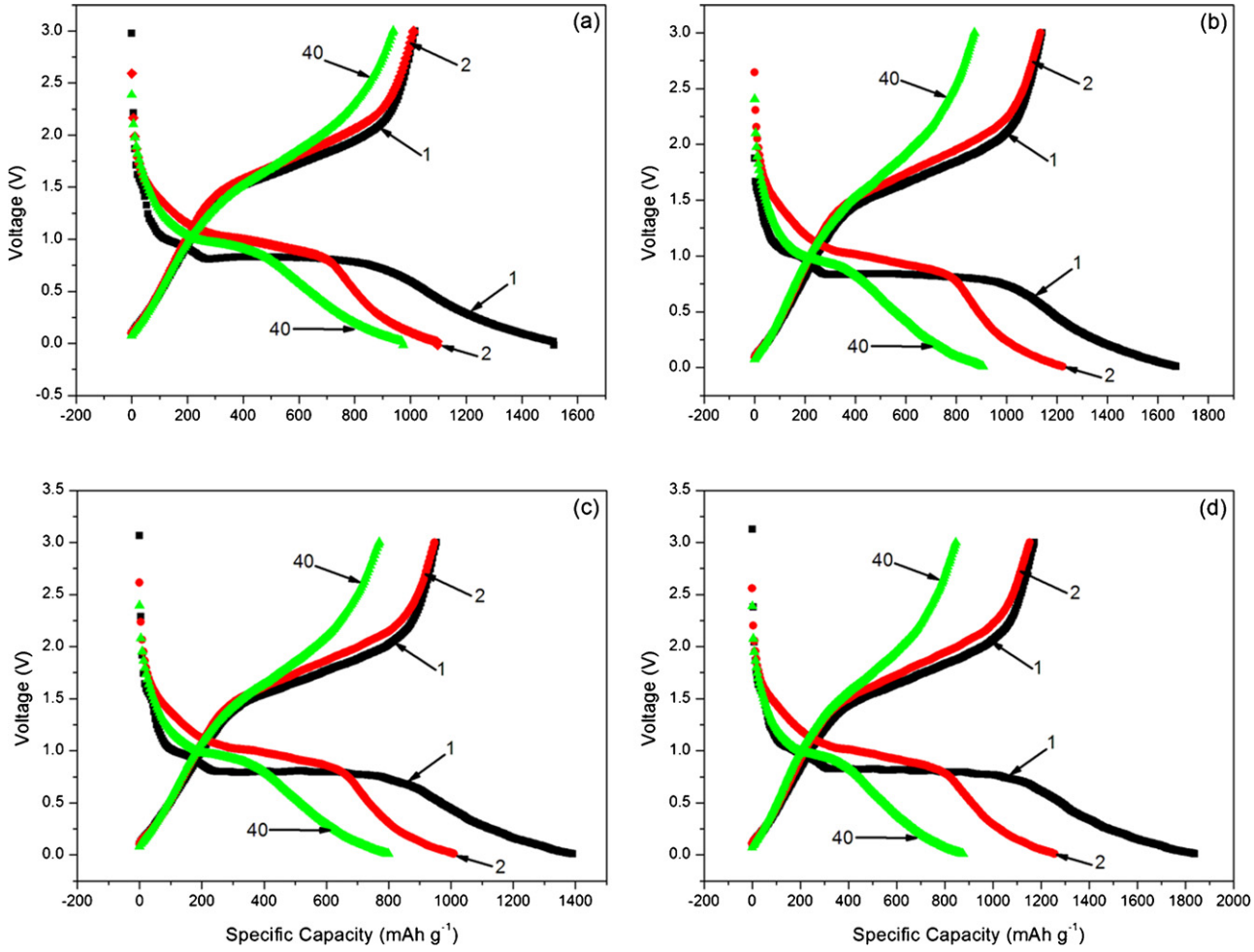

Fig. 5. The discharge and charge profiles of α-Fe_2O_3/Li half cells: (a) F02, (b) F04, (c) F06, and (d) F08 in the voltage range 0.01–3.0 V at a current density of 312.5 mA g^{-1}. The cycle numbers are indicated in the graphs.

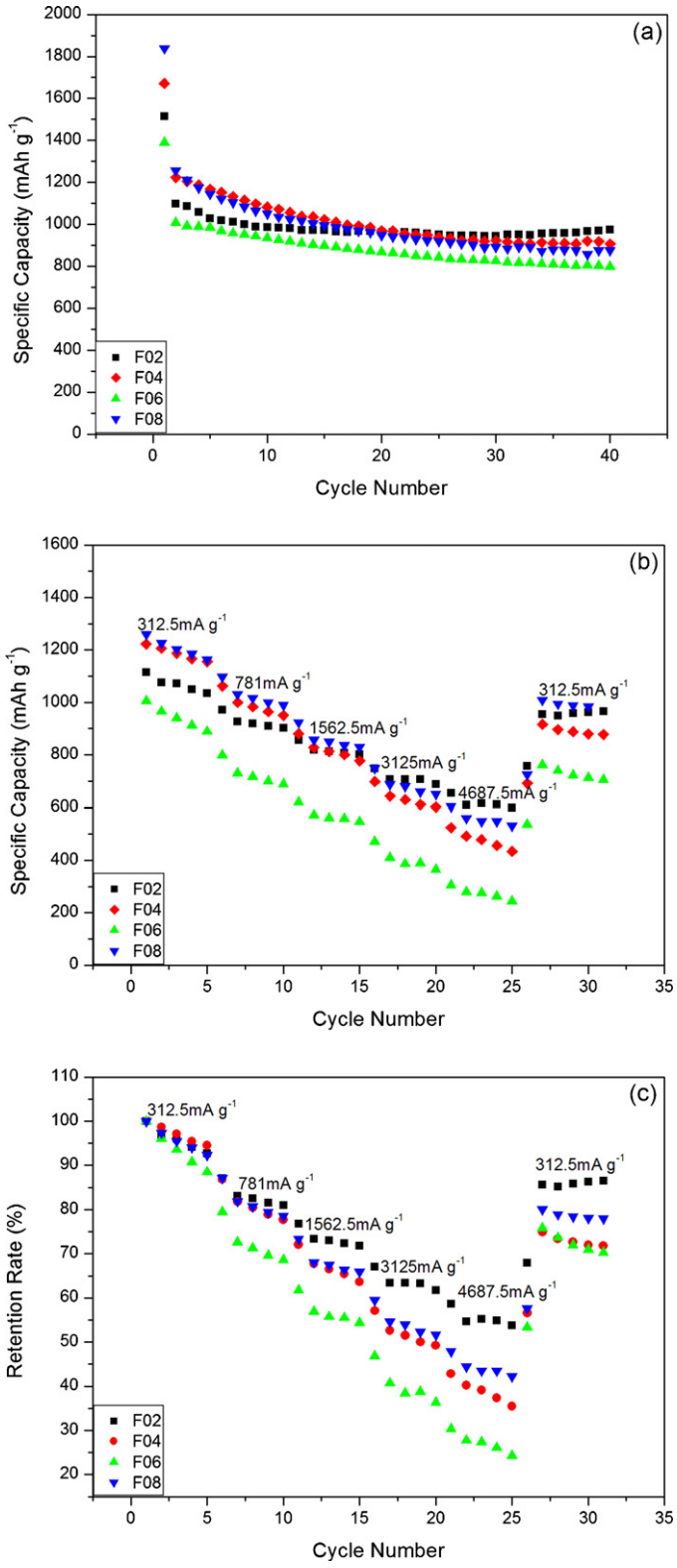

Fig. 6. Electrochemical properties of α-Fe_2O_3 clusters: (a) cycle performance of the electrodes at a current rate of 312.5 mA g^{-1}; (b) rate performance of the electrodes at different current density; (c) the capacity retention rate with respect to the discharge capacity of the second cycle at different current densities.

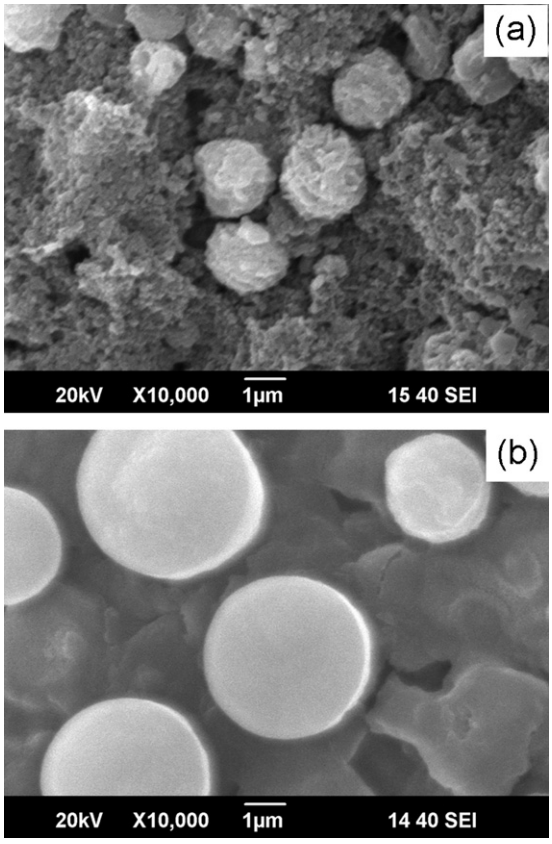

Fig. 7. SEM images of the electrodes prepared with F02 after 40 cycles at a current density of 312.5 mA g^{-1}: (a) charged to 3.0 V; (b) discharged to 0.01 V.

made of non-porous particles, of the above α-Fe_2O_3 electrodes is better in the kinetic performance. Their intercalation and extraction processes are of much higher efficiency so that a good cycling performance of the electrodes can be obtained. Besides, the porous structure can partially accommodate the volume change during the charge/discharge process. Among these four samples, F02 exhibits the best cycling performance that a specific capacity of 978 mAh g^{-1} can be obtained after 40 cycles; this result should be attributed to its largest specific surface area and more open structure.

In addition to the high capacity, the rate capability is also very important for the lithium-ion batteries in the practical application. Fig. 6b shows the rate performance of the α-Fe_2O_3 electrodes at various current densities from 312.5 mA g^{-1} to 4687.5 mA g^{-1}. It can be easily seen that F02 also has the best rate performance, exhibiting a high capacity of 928.5, 819.1, 712.9, and 622.1 mAh g^{-1} (about 55% of the second-cycle discharge capacity) at 781, 1562.5, 3125, and 4687.5 mA g^{-1}, respectively. When the charge current density returns to 312.5 mA g^{-1}, it can also deliver a high reversible capacity of 978.3 mAh g^{-1}. For other three samples, their discharge capacities are markedly decline with increasing the current density. Although F04 and F08 have higher rate capacity than that of F02 at 312.5, 781, and 1562.5 mA g^{-1}, F02 has the highest capacity retention rate with respect to the discharge capacity of the second cycle at various current densities from 781 to 4687.5 mA g^{-1}, as shown in Fig. 6c. All these results show that F02 displays both outstanding cycling performance and rate capability.

Furthermore, we examine the morphologies of the F02 after galvanostatic discharge–charge tests (Fig. 7). When charged to 3.0 V, the electrode has not change much relative to the as-prepared F02, it remains spherical and lamellar structure. When discharged to 0.01 V, the electrode still remains spherical, but becomes dense and smooth, it is mainly due to the formation of the Li_2O after

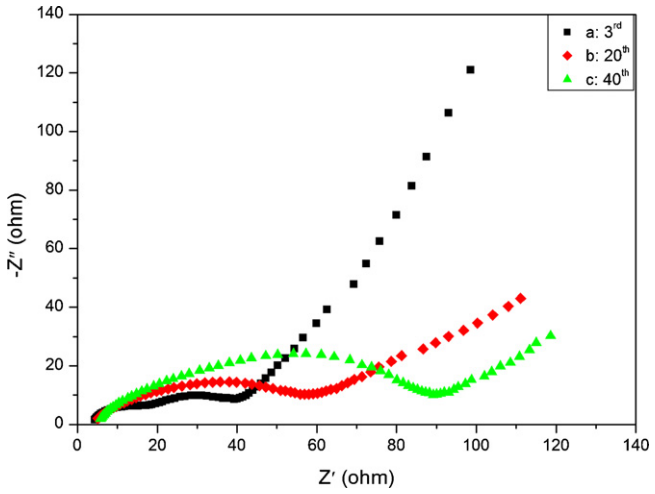

Fig. 8. Impedance spectra at the open-circuit voltage of 3.0 V after some electrochemical cycles at a current density of 312.5 mA g^{-1}: (a) 3rd; (b) 20th; (c) 40th.

the conversion reaction during the discharge process. These results demonstrate that the F02 with an open porous structure can accommodate the volumetric expansion and good to maintain the original structure and morphology, so it has a higher reversible capacity and better cycle performance.

The impedance spectra of the F02 at the end of the charge in 3rd, 20th, 40th cycle and at the end of the discharge in 40th cycle are shown in Fig. 8. The plots are similar to each other in shape, with one small semicircle appearing in the high frequency domain and one big semicircle in the medium region and a straight line in the low frequency region. It is clear that after 40th cycles at the open-circuit voltage of 3.0 V, the cell impedance increases substantially compared to its initial cycles. The change is likely due to the decomposition of the electrolyte during the cycling process.

4. Conclusions

In this paper, we have used a simple and efficient synthetic method and successfully prepared monodispersed porous α-Fe_2O_3 cluster powders. Their particle morphology can be easily tailored through changing the concentration of the precursor solution. The as-prepared samples are used as anode materials for lithium-ion batteries and show stable cycling performance with improved rate capability. In particular, the sample made from 0.02 M precursor solution with the highest specific surface area and the smallest cluster size exhibits the best electrochemical performance with high rate capability and reversible cycling performance. This synthesis method also provides a way to prepare other metal oxides as the anode materials for high performance lithium-ion batteries.

Acknowledgments

This study was supported by National Science Foundation of China (Grant Nos. 20971117, 10979049 and J1030412) and Education Department of Anhui Province (Grant No. KJ2009A142). We are also grateful to the Solar Energy Operation Plan of Academia Sinica.

References

[1] M. Armand, J.M. Tarascon, Building better batteries, Nature 451 (2008) 652.
[2] P.G. Bruce, B. Scrosati, J.M. Tarascon, Nanomaterials for rechargeable lithium batteries, Angewandte Chemie International Edition 47 (2008) 2930.
[3] J. Chen, L. Xu, W. Li, X. Gou, α-Fe_2O_3 nanotubes in gas sensor and lithium-ion battery applications, Advanced Materials 17 (2005) 582.
[4] S. Mita, P. Poizot, A. Finke, J.M. Tarascon, Growth and electrochemical characterization versus lithium of Fe_3O_4 electrodes made via electrodeposition, Advanced Functional Materials 16 (2006) 2281.
[5] I. Uzunov, S. Uzunova, D. Kovacheva, S. Vasilev, B. Puresheva, Iron-based composite oxides as alternative negative electrodes for lithium-ion batteries, Journal of Materials Science 42 (2007) 3353.
[6] P.C. Wang, H.P. Ding, T. Bark, C.H. Chen, Nanosized α-Fe_2O_3 and Li–Fe composite oxide electrodes for lithium-ion batteries, Electrochimica Acta 52 (2007) 6650.
[7] X.L. Wu, Y.G. Guo, L.J. Wan, C.W. Hu, Alpha-Fe_2O_3 nanostructures: INorganic salt-controlled synthesis and their electrochemical performance toward lithium storage, Journal of Physical Chemistry C 112 (2008) 16824.
[8] W.J. Yu, P.X. Hou, L.L. Zhang, F. Li, C. Liu, H.M. Cheng, Preparation and electrochemical property of Fe_2O_3 nanoparticles-filled carbon nanotubes, Chemical Communications 46 (2010) 8576.
[9] H. Duan, J. Gnanarj, X. Chen, B. Li, J. Liang, Fabrication and characterization of Fe_3O_4-based Cu nanostructured electrode for Li-ion battery, Journal of Power Sources 185 (2008) 512.
[10] Q. Pan, K. Huang, S. Ni, F. Yang, S. Lin, D. He, Synthesis of alpha-Fe_2O_3 dendrites by a hydrothermal approach and their application in lithium-ion batteries, Journal of Physics D: Applied Physics 42 (2009) 015417.
[11] D. Larcher, C. Masquelier, D. Bonnin, Y. Chabre, V. Masson, J.B. Leriche, J.M. Tarascon, Tarascon, effect of particle size on lithium intercalation into alpha-Fe_2O_3, Journal of the Electrochemical Society 150 (2003) A133.
[12] D. Larcher, D. Bonnin, R. Cortes, I. Rivals, L. Personnaz, J.M. Tarascon, Tarascon, Combined XRD, EXAFS, and Mossbauer studies of the reduction by lithium of alpha-Fe_2O_3 with various particle sizes, Journal of the Electrochemical Society 150 (2003) A1643.
[13] G.X. Wang, X.L. Gou, J. Horvat, J. Park, Facile synthesis and characterization of iron oxide semiconductor nanowires for gas sensing application, Journal of Physical Chemistry C 112 (2008) 15220.
[14] A.A. Tahir, K.G.U. Wijayantha, S. Saremi-Yarahmadi, M. Mazhar, V. McKee, Nanostructured (alpha-Fe_2O_3) thin films for photoelectrochemical hydrogen generation, Chemistry of Materials 21 (2009) 3763.
[15] Z.C. Wu, K. Yu, S.D. Zhang, Y. Xie, Hematite hollow spheres with a mesoporous shell: controlled synthesis and applications in gas sensor and lithium ion batteries, Journal of Physical Chemistry C 112 (2008) 11307.
[16] K. Woo, H.J. Lee, J.P. Ahn, Y.S. Park, Sol-gel mediated synthesis of Fe_2O_3 nanorods, Advanced Materials 15 (2003) 1761.
[17] L. Wang, H.W. Xu, P.C. Chen, D.W. Zhang, C.X. Ding, C.H. Chen, Electrostatic spray deposition of porous Fe_2O_3 thin films as anode material with improved electrochemical performance for lithium–ion batteries, Journal of Power Sources 193 (2009) 846.
[18] J.B. Lian, X.C. Duan, J.M. Ma, P. Peng, T.I. Kim, W.J. Zheng, Hematite (alpha-Fe_2O_3) with various morphologies: ionic liquid-assisted synthesis, formation mechanism, and properties, ACS Nano 3 (2009) 3749.
[19] J.P. Liu, Y.Y. Li, H.J. Fan, Z.H. Zhu, J. Jiang, R.M. Ding, Y.Y. Hu, X.T. Huang, Iron oxide-based nanotube arrays derived from sacrificial template-accelerated hydrolysis: large-area design and reversible lithium storage, Chemistry of Materials 22 (2010) 212.
[20] S.Q. Wang, J.Y. Zhang, C.H. Chen, Dandelion-like hollow microspheres of CuO as anode material for lithium-ion batteries, Scripta Materialia 57 (2007) 337.
[21] D. Larcher, G. Sudant, R. Patrice, J.M. Tarascon, Some insights on the use of polyols-based metal alkoxides powders as precursors for tailored metal-oxides particles, Chemistry of Materials 15 (2003) 3543.
[22] L.S. Zhong, J.S. Hu, H.P. Liang, A.M. Cao, W.G. Song, L.J. Wan, Self-assembled 3D flowerlike iron oxide nanostructures and their application in water treatment, Advanced Materials 18 (2006) 2426.
[23] S.W. Cao, Y.J. Zhu, M.Y. Ma, L. Li, L. Zhang, Hierarchically nanostructured magnetic hollow spheres of Fe_3O_4 and γ-Fe_2O_3: preparation and potential application in drug delivery, Journal of Physical Chemistry C 112 (2008) 1851.
[24] J.S. Xu, Y.Z. Zhu, Microwave-assisted ionic liquid solvothermal rapid synthesis of hollow microspheres of alkaline earth metal fluorides (MF_2, M = Mg, Ca, Sr), CrystEngComm 14 (2012) 2707.
[25] M. Rosso, C. Brissot, A. Teyssot, M. Dolle, L. Sannier, J.M. Tarascon, R. Bouchetc, S. Lascaud, Dendrite short-circuit and fuse effect on Li/polymer/Li cells, Electrochimica Acta 51 (2006) 5334.
[26] Y. Yu, C.H. Chen, J.L. Shui, S. Xie, Nickel-foam-supported reticular CoO–Li_2O composite anode materials for lithium ion batteries, Angewandte Chemie International Edition 44 (2005) 7085.
[27] L. Taberna, S. Mitra, P. Poizot, P. Simon, J.M. Tarascon, High rate capabilities Fe_3O_4-based Cu nano-architectured electrodes for lithium-ion battery applications, Nature Materials 5 (2006) 567.
[28] S. Grugeon, S. Laruelle, L. Dupont, J.M. Tarascon, An update on the reactivity of nanoparticles Co-based compounds towards Li, Solid State Sciences 5 (2003) 895.
[29] J.L. Shui, S.L. Zhang, W.L. Liu, Y. Yu, G.S. Jiang, S. Xie, C.F. Zhu, C.H. Chen, Exploration of alnico alloy as a magnetic electrode material for lithium-ion batteries, Electrochemistry Communications 6 (2004) 33.
[30] S. Laruelle, S. Grugeon, P. Poizot, M. Dolle, L. Dupont, J.M. Tarascon, On the origin of the extra electrochemical capacity displayed by MO/Li cells at low potential, Journal of the Electrochemical Society 149 (2002) A627.